

## RESEARCH ARTICLE

10.1002/2014JD021911

## Key Points:

- Proper handling of IASI-NH<sub>3</sub> retrieval error is key for model evaluation
- Modeled and retrieved European NH<sub>3</sub> distributions are largely consistent
- Need for improvement of emission pattern in time and space highlighted

## Supporting Information:

- Text S1
- Animation S1

## Correspondence to:

M. Van Damme,  
Martin.Van.Damme@ulb.ac.be

## Citation:

Van Damme, M., R. J. Wichink Kruit, M. Schaap, L. Clarisse, C. Clerbaux, P.-F. Coheur, E. Dammers, A. J. Dolman, and J. W. Erisman (2014), Evaluating 4 years of atmospheric ammonia (NH<sub>3</sub>) over Europe using IASI satellite observations and LOTOS-EUROS model results, *J. Geophys. Res. Atmos.*, 119, doi:10.1002/2014JD021911.

Received 15 APR 2014

Accepted 5 JUL 2014

Accepted article online 9 JUL 2014

## Evaluating 4 years of atmospheric ammonia (NH<sub>3</sub>) over Europe using IASI satellite observations and LOTOS-EUROS model results

M. Van Damme<sup>1,2</sup>, R. J. Wichink Kruit<sup>3</sup>, M. Schaap<sup>3</sup>, L. Clarisse<sup>1</sup>, C. Clerbaux<sup>1,4</sup>, P.-F. Coheur<sup>1</sup>, E. Dammers<sup>2,3</sup>, A. J. Dolman<sup>2</sup>, and J. W. Erisman<sup>2,5</sup>

<sup>1</sup>Spectroscopie de l'atmosphère, Chimie Quantique et Photophysique, Université Libre de Bruxelles, Brussels, Belgium,

<sup>2</sup>Cluster Earth and Climate, Department of Earth Sciences, Vrije Universiteit Amsterdam, Amsterdam, Netherlands,

<sup>3</sup>Department of Climate, Air and Sustainability, TNO, Utrecht, Netherlands, <sup>4</sup>Sorbonne Universités, UPMC Univ. Paris 06; Université Versailles St.-Quentin; CNRS/INSU, LATMOS-IPSL, Paris, France, <sup>5</sup>Louis Bolk Institute, Driebergen, Netherlands

**Abstract** Monitoring ammonia (NH<sub>3</sub>) concentrations on a global to regional scale is a challenge. Due to the limited availability of reliable ground-based measurements, the determination of NH<sub>3</sub> distributions generally relies on model calculations. Novel remotely sensed NH<sub>3</sub> burdens provide valuable insights to complement traditional assessments for clear-sky conditions. This paper presents a first quantitative comparison between Atmospheric Sounding Interferometer (IASI) satellite observations and LOTOS-EUROS model results over Europe and Western Russia. A methodology to account for the variable retrieval sensitivity of the measurements is described. Four years of data (2008–2011) highlight three main agricultural hot spot areas in Europe: the Po Valley, the continental part of Northwestern Europe, and the Ebro Valley. The spatial comparison reveals a good overall agreement of the NH<sub>3</sub> distributions not only in these source regions but also over remote areas and over sea when transport is observed. On average, the measured columns exceed the modeled ones, except for a few cases. Large discrepancies over several industrial areas in Eastern Europe and Russia point to underestimated emissions in the underlying inventories. The temporal analysis over the three hot spot areas reveals that the seasonality is well captured by the model when the lower sensitivity of the satellite measurements in the colder months is taken into account. Comparison of the daily time series indicates possible misrepresentations of the timing and magnitude of the emissions. Finally, specific attention to biomass burning events shows that modeled plumes are less spread out than the observed ones. This is confirmed for the 2010 Russian fires with a comparison using in situ observations.

### 1. Introduction

Ammonia (NH<sub>3</sub>) is a key component in our ecosystems [Sutton *et al.*, 2013]. As the primary form of reactive nitrogen in the environment, it plays an important role in nitrogen deposition and the associated eutrophication and acidification [Erisman *et al.*, 2007; Zhang *et al.*, 2012]. Once emitted in the atmosphere, NH<sub>3</sub> is highly relevant as it is the major atmospheric base that neutralizes atmospheric acids (e.g., sulfuric acid and nitric acid). NH<sub>3</sub> can in this way also contribute to particulate matter formation, providing a means of long-range transport for reactive nitrogen [Erisman *et al.*, 2007; Hertel *et al.*, 2012]. The significant effect of NH<sub>3</sub> on particulate matter has been demonstrated using model simulations [Erisman and Schaap, 2004; Heald *et al.*, 2012; Gong *et al.*, 2013; Schiferl *et al.*, 2014] and in situ campaigns [Nowak *et al.*, 2012; Gong *et al.*, 2013]. This role in secondary inorganic aerosol formation affects climate and air quality and as a result human and ecosystem health [Erisman *et al.*, 2008, 2013; Pope *et al.*, 2009; Adams *et al.*, 2013; Paulot and Jacob, 2014]. Despite ongoing research, NH<sub>3</sub> is still the reactive nitrogen compound with the largest uncertainties in the nitrogen cycle [Fowler *et al.*, 2013].

Perturbations of the nitrogen cycle and NH<sub>3</sub> emissions in particular strongly increased during the twentieth century following demand for food of an ever growing population [Erisman *et al.*, 2008]. Globally, NH<sub>3</sub> is mainly emitted by agricultural activities and biomass burning [Emission Database for Global Atmospheric Research, 2011]. Other sources such as traffic and industry can be important contributors on regional scales [Reis *et al.*, 2009]. According to the European Environment Agency [European Environment Agency (EEA), 2012] the dominant sector in Europe is also agriculture, representing 97.3% of the emissions in 2010

(including field burning of agricultural waste), followed by the waste sector (2.1%). In the past decades  $\text{NH}_3$  emissions have been somewhat declining in Europe, following improvements in manure management and a decrease in fertilizer use and livestock [EEA, 2012].

Spatial  $\text{NH}_3$  distributions can be obtained via chemistry transport models (CTMs). As  $\text{NH}_3$  is short lived and spatially highly disperse, model results are very dependent on the timing and gridding of the emissions used as input. These gridded emissions are typically obtained by redistributing in time and space the nationally reported yearly total emissions [Pouliot *et al.*, 2012]. Such an allocation is nontrivial due to dependency of emissions on local activity levels (agricultural and industrial) linked with environmental conditions (e.g., temperature, relative humidity, soil pH, and total ammoniacal nitrogen content) [Bouwman *et al.*, 2002; Velthof *et al.*, 2012]. Although first attempts have been made to model  $\text{NH}_3$  emissions dynamically [Skjøth *et al.*, 2011; Hamaoui-Laguel *et al.*, 2014], CTMs generally account for the spatiotemporal variations in a simplified way [Hutchings *et al.*, 2001; van Pul *et al.*, 2009]. The usual approach is to combine emission factors and activity data and weight those with a fixed temporal profile (monthly, daily, and/or hourly resolved) [van Pul *et al.*, 2009].

Until recently, the only way in which  $\text{NH}_3$  model results could be evaluated was by comparison with ground-based measurements. These are, however, technically challenging [von Bobrzki *et al.*, 2010], and in Europe only few stations provide daily or hourly  $\text{NH}_3$  measurements.  $\text{NH}_3$  concentrations are mostly monitored with passive samplers or dedicated denuder filter packs with sampling periods covering 1, 2, or 4 weeks [Sutton *et al.*, 2007; Flechard *et al.*, 2011]. Moreover, the resulting data are often not representative for the corresponding much larger grid cells in CTMs making a detailed model evaluation challenging [Wichink Kruit *et al.*, 2012a]. Recently, infrared satellites characterized by a high spatial and temporal sampling were shown capable of probing  $\text{NH}_3$  in the lower troposphere [Clarisse *et al.*, 2009, 2010; Shephard *et al.*, 2011; Van Damme *et al.*, 2014]. Spaceborne measurements have the additional advantage of offering area averaged observations which are in much better correspondence with the size of the grid cells in regional/global models [Flechard *et al.*, 2013].

The first observations of  $\text{NH}_3$  from space were made with the Tropospheric Emission Spectrometer (TES) instrument [Beer *et al.*, 2008]. Another instrument able of measuring this trace gas is the Infrared Atmospheric Sounding Interferometer (IASI) [Coheur *et al.*, 2009]. As a meteorological satellite, it has a much better spatial and temporal coverage than TES [Clerbaux *et al.*, 2009; Streets *et al.*, 2013]. First global  $\text{NH}_3$  distributions and model comparisons were obtained with this instrument [Clarisse *et al.*, 2009]. In that study the model simulations from the Tracer Model 5 (TM5) revealed underestimates in  $\text{NH}_3$  inventories, especially in central Asia. Shephard *et al.* [2011] made initial comparisons between TES observations and GEOS-Chem model results and found that measured columns were overall higher than modeled ones. Several other studies using the available space measurements investigated anthropogenic dust [Ginoux *et al.*, 2012], particulate matter [Heald *et al.*, 2012; Walker *et al.*, 2012], and spatial and seasonal variability of  $\text{NH}_3$  [Clarisse *et al.*, 2010; Pinder *et al.*, 2011; Kharol *et al.*, 2013]. First inverse modeling work using TES observations have highlighted the underestimation of emission inventories particularly in the west of the United States [Zhu *et al.*, 2013].

At present, there are no detailed studies analyzing the performance of CTMs on regional scales using high spatiotemporal resolved measurements. Here we use IASI satellite and LOTOS-EUROS model data to analyze the distribution, the interannual and intraannual variability of  $\text{NH}_3$  and compare the model on such scales with the satellite observations. We focus on the European region using LOTOS-EUROS simulations, complementing in part the satellite model studies focusing on the United States. In the next section we present the IASI instrument, the  $\text{NH}_3$  retrieval method, and the LOTOS-EUROS model, and finally, we describe the regularization methodology which allows taking into account the variable sensitivity of satellite measurements to  $\text{NH}_3$ . In section 3, we analyze and compare the measurements with the model simulations over Europe.

## 2. Method

In this study we considered IASI observations and LOTOS-EUROS simulations from 1 January 2008 to 31 December 2011. The study area over Europe is taken between  $-15^\circ\text{E}$  and  $55^\circ\text{E}$ , and  $35^\circ\text{N}$  and  $70^\circ\text{N}$ . This domain is larger than the default model domain of LOTOS-EUROS which was extended eastward to capture the  $\text{NH}_3$  emissions from the Russian fires in 2010.

**Table 1.** IASI-NH<sub>3</sub> Measurement Availability for 2011<sup>a</sup>

	Jan	Feb	Mar	Apr	May	Jun	Jul	Aug	Sep	Oct	Nov	Dec	2011
All (cloud free)	75,219	69,249	156,302	168,084	143,956	174,980	191,908	198,269	168,725	139,652	101,176	73,989	1,669,317
Error below 50%	2,937	4,356	19,215	41,638	42,364	38,888	40,322	42,330	31,251	15,718	5,141	4,148	288,308

<sup>a</sup>Number of cloud-free IASI measurements (cloud coverage below 25%) over Europe (−15°E to 55°E and 35°N to 70°N) and corresponding number of cloud-free IASI measurements with a retrieval error smaller than 50% per month in 2011.

### 2.1. NH<sub>3</sub> From IASI

IASI is a passive remote-sensing instrument operating in nadir mode (downward vertically viewing geometry) and measures the infrared radiation emitted by the Earth surface and the atmosphere in the 645–2760 cm<sup>−1</sup> spectral range [Clerbaux *et al.*, 2009]. This instrument, the first of a series of three, was launched in 2006 on board the MetOp-A meteorological platform which circles in a polar Sun-synchronous orbit. It crosses the equator at a mean local solar time of 9:30 A.M. and P.M. (hereafter referred to as daytime and nighttime measurements), corresponding to a measurement time range between 7 and 12 UTC for the domain of interest, and has an elliptical footprint of 12 by 12 km up to 20 by 39 km depending on the satellite viewing angle. IASI has already proved to be an invaluable instrument for monitoring atmospheric composition owing to its spectral performances and high spatiotemporal sampling [Hilton *et al.*, 2012]. In this study we use daytime satellite observations as these are more sensitive to NH<sub>3</sub> [Van Damme *et al.*, 2014].

An improved retrieval scheme for IASI spectra was recently presented in Van Damme *et al.* [2014]. It relies on the calculation of a dimensionless “Hyperspectral Range Index”, which is subsequently converted to a total NH<sub>3</sub> column. This step is performed using look-up tables built from forward radiative transfer simulations. These simulations have been done using only two profile shapes: one for all measurement above land and another one for all those above sea. The bias introduced by considering fixed profile shapes in the retrieval scheme is expected to be not higher than a factor of 2 in the majority of cases, as explained in Van Damme *et al.* [2014]. The retrieval method combines a good sensitivity to NH<sub>3</sub> with computational advantages, allowing the processing of large amounts of observations. In addition, in comparison to previous IASI algorithms (e.g., as in Heald *et al.* [2012]), the improved retrieval method significantly increases the amount of daily successful retrievals. The algorithm also allows quantitative error estimates of individual observations. As the measurement accuracy of NH<sub>3</sub> is very variable, it needs to be properly taken into account to compare with independent data (see section 2.3). The sensitivity of NH<sub>3</sub> space measurements mainly depends on the thermal contrast (which is the temperature difference between the Earth surface and the atmosphere at 1.5 km) and the amount of NH<sub>3</sub>.

As an illustration of the measurement availability, we report here some measurement statistics for 2011. A total number of 1,669,317 cloud-free daytime observations (considering a cloud coverage below 25%, as characterized by the operational IASI processor [see August *et al.*, 2012]) were retrieved over land in the study domain. From those observations, 288,308 measurements have an estimated error below 50% (see Table 1). The monthly values, also reported in Table 1, show that winter months (December–January–February (DJF)) represent only 13% of the data set in 2011, while spring (March–April–May (MAM)), summer (June–July–August (JJA)), and autumn (September–October–November (SON)) represent 28%, 34%, and 25%, respectively. Of the observations with an error smaller than 50%, only 4% are in DJF, 36% are in MAM, 42% are in JJA, and 18% are in SON. Spring and summer thus account for 78% of all 2011 observations with errors lower than 50%. The number of observations per month in the data set is therefore mainly affected by the cloud coverage, while the number of observations per month with a retrieval error smaller than 50% is affected by the thermal contrast and the amount of NH<sub>3</sub> present. The NH<sub>3</sub> retrieval algorithm relies on the use of collocated geophysical parameters, specifically the surface temperature and the air temperature at 1.5 km, which are provided in the Level 2 (L2) IASI data. Atmospheric temperature profiles are essential for the calculation of the thermal contrast [Van Damme *et al.*, 2014]. The quality of the retrieval increased in the course of 2010 because of improvements in the L2 data. In particular, after 3 March 2010, L2 information was for the first time provided for all IASI observations (before this was the case for one in two observations) [Dufour *et al.*, 2012]. In addition, on 14 September 2010 an improved version of the L2 was introduced, characterized by improvements in the temperature profile (especially in the troposphere), cloud properties products, and cloud detection [August *et al.*, 2012].

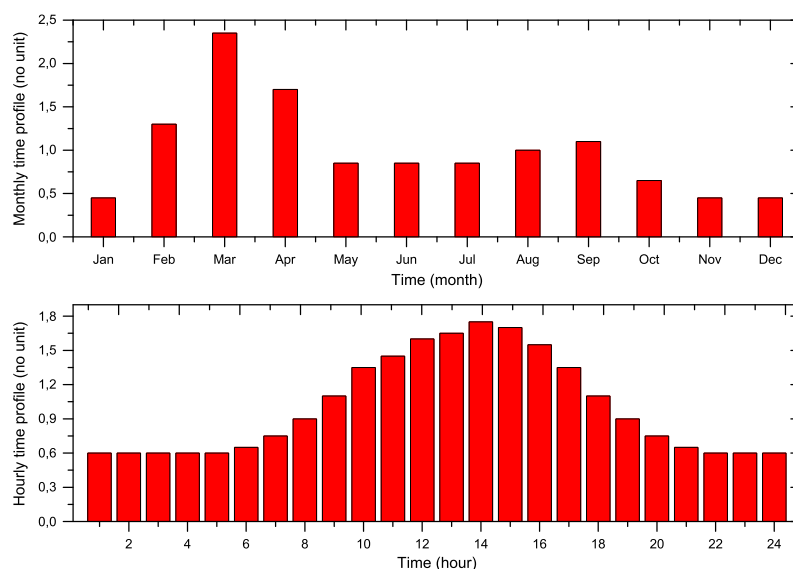


**Figure 1.** Fixed temporal profile for agricultural emissions used in LOTOS-EUROS (no unit). (top) Monthly time profile. (bottom) Hourly time profile.

## 2.2. LOTOS-EUROS Model

The LOTOS-EUROS model is a regional CTM, which simulates air pollution in the lowest 3.5 km of the troposphere [Schaap *et al.*, 2008]. All relevant processes in the atmosphere are parameterized in such a way that the computational demands are not too large, such that hour-by-hour calculations over extended periods of several years are still possible within acceptable CPU time of several days. In this study we used LOTOS-EUROS version 1.8. In this version of the model, the ISORROPIA II aerosol chemistry routine is used to convert  $\text{NH}_3$  into ammonium aerosol [Fountoukis and Nenes, 2007]. This model version also includes a pH-dependent cloud chemistry scheme following Banzhaf *et al.* [2012]. Wet deposition of trace gases and aerosols are treated using simple scavenging coefficients for gases [Schaap *et al.*, 2004a] and particles [Simpson *et al.*, 2003]. Formation of coarse-mode nitrate is included in a dynamical way [Wichink Kruit *et al.*, 2012b]. The surface-atmosphere exchange of gases is parameterized following the well-known resistance approach using the updated DEPAC scheme, i.e., DEPosition of Acidifying Compounds, which includes canopy compensation points for  $\text{NH}_3$  [van Zanten *et al.*, 2010]. The deposition of particles is represented by the methodology of Zhang *et al.* [2001].

The geographic projection is equirectangular with a standard grid resolution of  $0.50^\circ$  longitude by  $0.25^\circ$  latitude, approximately 28 by 28 km at the latitude under consideration here. The actual domain for a simulation can be set, and it is possible to increase or decrease the resolution up to a factor 8 or 2, respectively. In the vertical, the model follows the well-mixed dynamic boundary layer concept. There are three dynamic layers and a surface layer. The lowest dynamic layer is the mixing layer, followed by two reservoir layers. The height of the mixing layer is obtained from the European Centre for Medium-Range Weather Forecasts meteorological input data used to drive the model. The height of the reservoir layers is determined by the difference between ceiling and mixing layer height. A surface layer with a fixed depth of 25 m is included as part of the mixing layer to monitor ground-level concentrations.

For the  $\text{NH}_3$  emissions (except from fires), the LOTOS-EUROS model relies on the Netherlands Organization for Applied Scientific Research (TNO) Monitoring Atmospheric Composition and Climate (MACC) European emission inventory for the year 2007 [Kuenen *et al.*, 2011] which is based on the high-resolution European emission data base for the year 2005 [Denier van der Gon *et al.*, 2010]. Reported  $\text{NH}_3$  emissions (European Monitoring and Evaluation Programme (EMEP)/Convention on Long-Range Transboundary Air Pollution (CRLTAP)) were distributed over countries using the animal numbers per square kilometer from the Food and Agriculture Organization Gridded Livestock of the World data set. For the timing of the emissions, fixed annual and daily time profiles were used as shown in Figure 1 [Denier van der Gon *et al.*, 2011].  $\text{NH}_3$  emissions from forest fires were included using the Global Fire Assimilation System (GFASv1.1) developed in the MACC-II project ([www.gmes-atmosphere.eu](http://www.gmes-atmosphere.eu)) [Andela *et al.*, 2013].

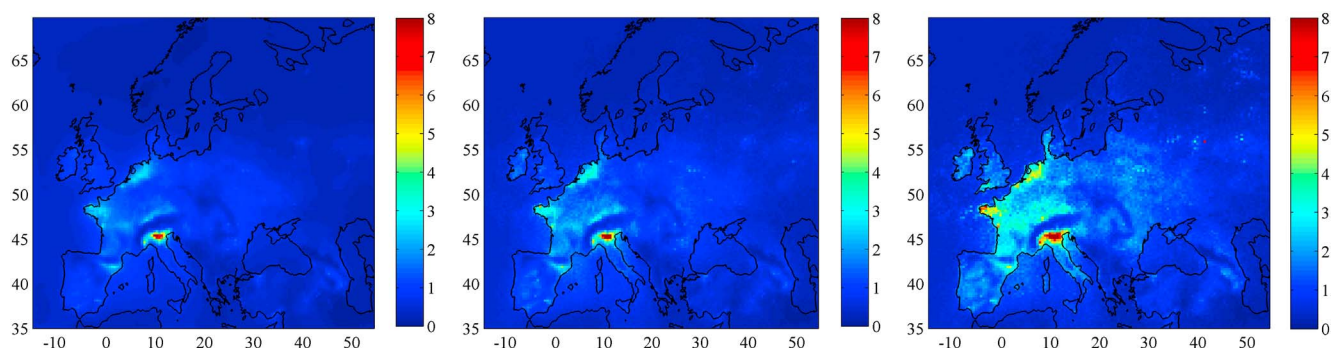


**Figure 2.** LOTOS-EUROS NH<sub>3</sub> total column (mg/m<sup>2</sup>) distributions for 2011: (left) arithmetic average of all hourly simulations of LOTOS-EUROS, (middle) arithmetic average using the sampling of IASI, (right) weighted and sampled average based on collocated IASI measurements and equation (1).

The LOTOS-EUROS model is one of the few CTMs that use a description of the bidirectional surface-atmosphere exchange of NH<sub>3</sub> [Wichink Kruit *et al.*, 2010, 2012a]. In general, the model results showed a good correspondence with yearly averaged NH<sub>3</sub> measured concentrations, e.g., slightly underestimating concentrations in agricultural source areas and slightly overestimating concentrations in nature areas [Wichink Kruit *et al.*, 2012a]. LOTOS-EUROS participated in two recent model intercomparison studies: ECLAIRE [Wichink Kruit *et al.*, 2013] and EURODELTA [Bessagnet *et al.*, 2013] and showed an overall good model performance. The emission patterns in space and time as well as a proper approach to deal with the high-concentration gradients in relation to model resolution were considered to be the biggest challenges.

### 2.3. Regularizing IASI and LOTOS-EUROS Columns

To compare modeled to measured NH<sub>3</sub> distributions, the variable sampling of the satellite needs to be taken into account, which is determined by the overpass time and the cloud coverage. A one-to-one correspondence was obtained by selecting for each IASI-NH<sub>3</sub> observation the LOTOS-EUROS simulation closest in time and space.

In addition to the sampling, the comparison of the IASI data set with independent observations or model results requires that retrieval errors are carefully taken into consideration. It is worth noting that differential measurement sensitivity in remote sensing is usually accounted for with the use of averaging kernels [Rodgers, 2000]. However, these are only available for constrained retrievals which rely on a priori information. The NH<sub>3</sub> retrieval algorithm applied here does not rely on any a priori information, and hence, no averaging kernels are available. To take retrieval sensitivity into account and in addition focus on those measurements with a low retrieval error, we have weighted both the model simulations and satellite measurements as [Van Damme *et al.*, 2014]

$$\bar{x} = \frac{\sum w_i x_i}{\sum w_i} \quad (1)$$

where  $w_i$  is the weighting factor equal to  $1/\sigma_i^2$  and  $\sigma_i$  is the relative error on the retrieved column,  $x_i$  being an IASI measurement or a LOTOS-EUROS simulation. Finally, the satellite data were gridded at the spatial resolution of the model. Equation (1) is also used to calculate the mean retrieval error  $\bar{\sigma}$  which can be assigned to each averaged observed column, in this case  $x_i$  becomes  $\sigma_i$  (the relative retrieval error on each observation). This equation is used for averaging several measurements over an area and/or over time.

Figure 2 shows LOTOS-EUROS simulated averaged distributions for 2011 and the effect of this regularization procedure. The left panel is an arithmetic mean of all hourly simulations. In the middle panel only those simulations collocated with IASI measurements are averaged. Finally, the right panel additionally takes into account the differential measurement sensitivity by applying equation (1) on the simulations. The systematically higher levels in the regularized distribution clearly show the influence of the overpass time of the satellite as well as the higher-quality retrievals available for fair weather conditions and higher NH<sub>3</sub> levels. These results highlight the necessity to treat the collocated modeled and measured column densities in the same way. In what follows all presented distributions have been weighted and sampled in this way. Also, total NH<sub>3</sub> columns reported hereafter should be interpreted as weighted columns.

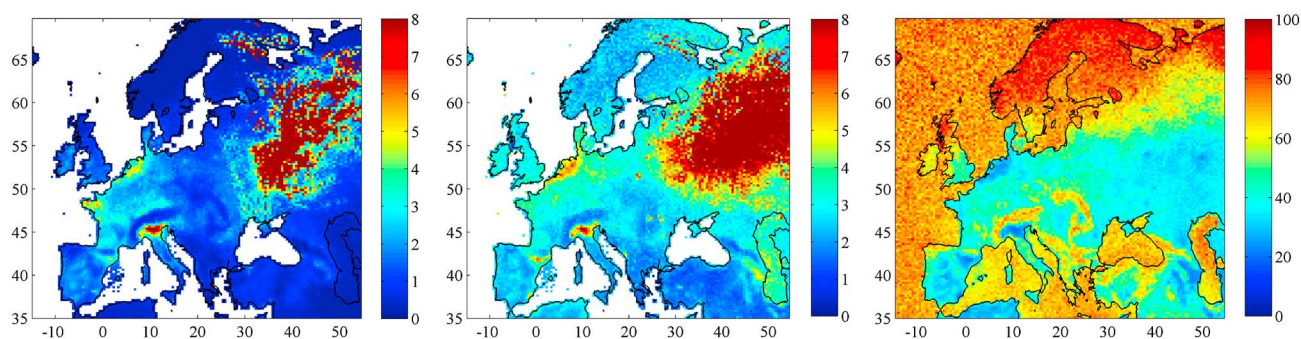


**Figure 3.** Four year averaged distributions of LOTOS-EUROS (left) modeled  $\text{NH}_3$  total columns ( $\text{mg}/\text{m}^2$ ), (middle) measured  $\text{NH}_3$  total columns by IASI ( $\text{mg}/\text{m}^2$ ), and (right) associated IASI-retrieved relative error (%).

### 3. Results

In this section we start by analyzing 4 year averaged geographical distributions of IASI and LOTOS-EUROS both over land and sea. Next, we study and analyze in detail the distributions of the individual years during this period. Also, the seasonal and day-to-day variability are investigated, and finally, the Russian fire episode in the summer of 2010 is briefly discussed.

#### 3.1. Four Year Mean

The averaged  $\text{NH}_3$  distributions derived from 4 years of monitoring (1 January 2008 to 31 December 2011) are shown in Figure 3. Left panel shows the total  $\text{NH}_3$  columns as modeled by LOTOS-EUROS ( $\text{mg}/\text{m}^2$ ). Middle and right panels show the IASI satellite observations:  $\text{NH}_3$  distributions (middle,  $\text{mg}/\text{m}^2$ ) and the associated relative errors (right, %). A postfiltering of the mean total  $\text{NH}_3$  columns above sea has been carried out on the unreliable observed cells (associated with a mean relative error above 58%), and the same filter was used on the modeled distribution. As expected, lowest 4 year mean errors around 20% are associated with  $\text{NH}_3$  hot spots. The highest column concentrations over East Europe are due to the exceptional  $\text{NH}_3$  emissions during the 2010 Russian fires [R'Honi *et al.*, 2013]. The particularly favorable conditions for  $\text{NH}_3$  infrared remote sensing of such fires lead to very small retrieval uncertainty and give this event a large weight in the total average distribution.

Overall, the IASI satellite-derived columns exceed the modeled columns. This is consistent with initial comparisons made globally between GEOS-Chem model and TES satellite observations [Shephard *et al.*, 2011]. The modeled and measured  $\text{NH}_3$  distributions in Figure 3 show the same important source areas: the Po Valley in Northern Italy, the continental part of northwestern Europe (in particular the Netherlands), and finally the Ebro Valley in Northern Spain. The Po Valley has 4 year average measured columns up to  $9.4 \text{ mg}/\text{m}^2$  (with an average retrieval error of 19%, calculated following equation (1)) and modeled columns up to  $13 \text{ mg}/\text{m}^2$ . This agricultural and industrial valley is the strongest emitter of  $\text{NH}_3$  in Europe [Clarisse *et al.*, 2009; Pouliot *et al.*, 2012; Skjoth *et al.*, 2011]. In the Netherlands, IASI average columns are as high as  $6.5 \text{ mg}/\text{m}^2$  (with an average retrieval error of 24%), while the model simulates  $\text{NH}_3$  columns up to  $5.2 \text{ mg}/\text{m}^2$ . This country is known for its intensive agriculture and associated high  $\text{NH}_3$  emissions. For the Ebro Valley, the model calculates  $\text{NH}_3$  columns up to  $5 \text{ mg}/\text{m}^2$ , while the satellite instrument measures columns up to  $6.3 \text{ mg}/\text{m}^2$  (with an average retrieval error of 21%). Remote areas show lower simulated concentrations than observed, but larger errors are associated with the observations (for example, in Northern or Eastern Europe), preventing us from drawing conclusions for these.

Although the error filtering of the data removes most of the distributions over sea, marked columns can be observed off the coasts of the Ebro and Po Valleys. The observed transport is reproduced by the model, aided by the improved modeling of  $\text{NH}_3$  over sea by using an updated deposition module (DEPAC3.11, see Wichink Kruit *et al.* [2012a]).

#### 3.2. Interannual Analysis

Figure 4 shows the yearly  $\text{NH}_3$  distributions for 2008, 2009, 2010, and 2011 (top to bottom) of the LOTOS-EUROS simulations ( $\text{mg}/\text{m}^2$ ), the IASI observations ( $\text{mg}/\text{m}^2$ ), and the associated mean retrieval error on the observations (%) and the difference between IASI and LOTOS-EUROS distribution ( $\text{mg}/\text{m}^2$ )

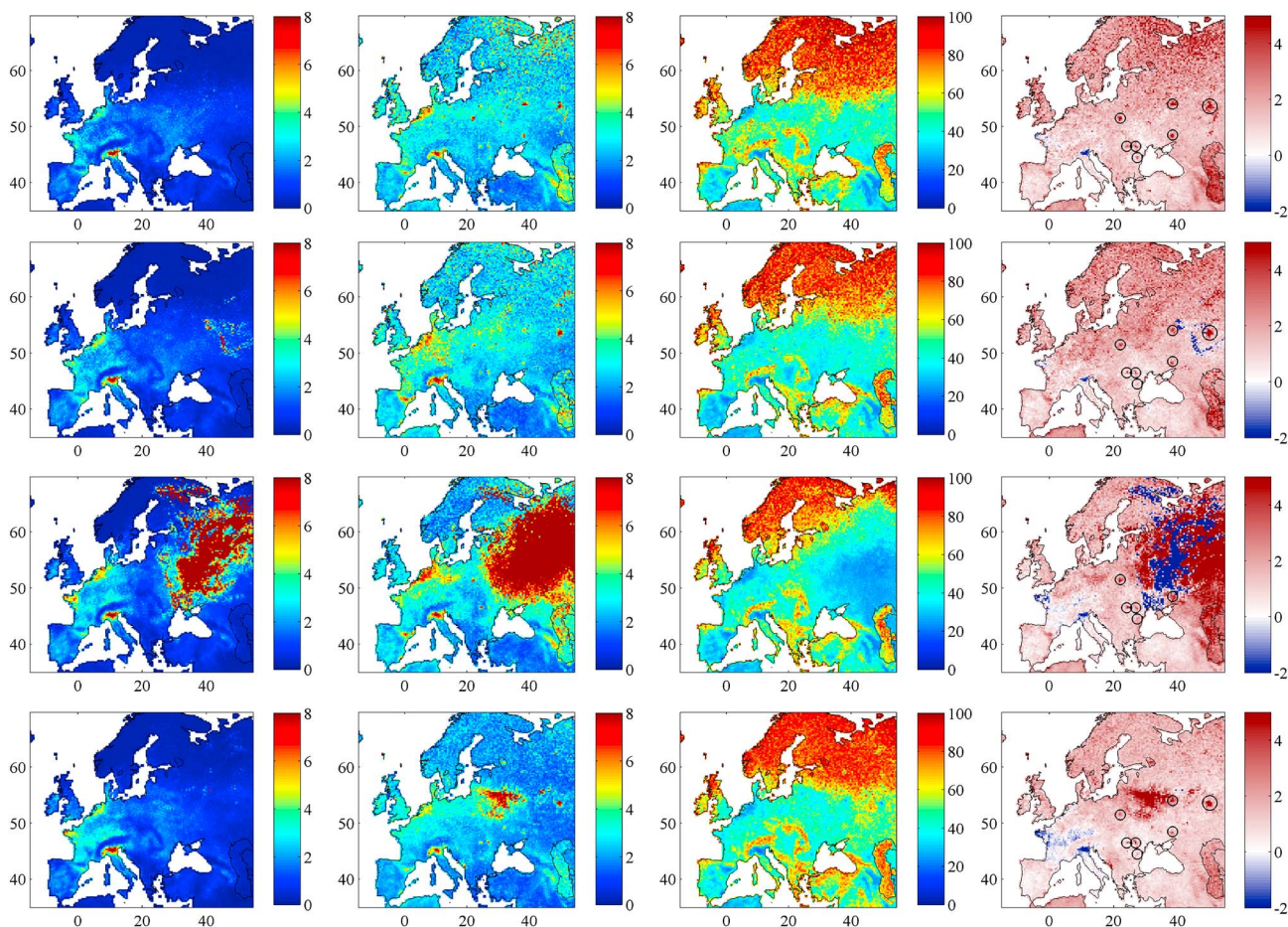


**Figure 4.** From left to right: the  $\text{NH}_3$  distribution modeled by LOTOS-EUROS ( $\text{mg}/\text{m}^2$ ), the  $\text{NH}_3$  distribution measured by the IASI satellite ( $\text{mg}/\text{m}^2$ ), the average relative retrieval error distribution (%), and the difference between IASI measurements and LOTOS-EUROS simulations ( $\text{mg}/\text{m}^2$ ); the black circles highlight the industrial hot spots of Table 2. From top to bottom: Each row corresponds to a yearly average from 2008 to 2011.

(left to right). The year 2010 stands out due to the large emissions from the fire episode in Russia, which was caused by the Northern Hemisphere summer heat wave of 2010 [Barriopedro *et al.*, 2011]. The heat wave apparently also impacted other parts of Europe as the columns over many of the hot spot areas in that year were higher than any other year (best seen in Figure 4 over the Netherlands), possibly due to the temperature dependence of  $\text{NH}_3$  volatilization [Sutton *et al.*, 2013]. For all 4 years, IASI observes generally higher yearly averaged columns than the ones simulated by LOTOS-EUROS. The averaged bias calculated over Europe for 2008, 2009, 2010, and 2011 equals 1.92, 1.86, 1.11, and 1.44  $\text{mg}/\text{m}^2$ , respectively. Note that 2010 is a special year to be excluded from this bias analysis due to the impact of the Russian fires, which are discussed in section 3.4. The decrease in the bias observed in 2011 could be explained in part by the quality improvement made on the IASI- $\text{NH}_3$  product (see section 2.1 and August *et al.* [2012]).

There are three regions where model simulations exceed the observed columns:

1. Brittany in the North of France, mainly in 2010 and 2011. The overestimation of the model in this region is consistent with a recent model study [Hamaoui-Laguel *et al.*, 2014]. There, a decrease of modeled emissions for this area was obtained by introducing an improved representation of the  $\text{NH}_3$  emissions from agricultural activities. So the high modeled  $\text{NH}_3$  columns in LOTOS-EUROS results are likely caused by an incorrect allocation of the  $\text{NH}_3$  emissions in the underlying MACC emission database.
2. The Po Valley in Italy. The low retrieval errors associated with the satellite observations suggest an overestimation of  $\text{NH}_3$  by the model. This valley is characterized both by intensive agriculture and industry. A possible explanation is therefore an underestimation of the emission of industrial pollutants

**Table 2.** Industrial Hot Spot Areas Identified by the Model/Satellite Comparison<sup>a</sup>

Site	Latitude (°N)	Longitude (°E)	Yearly Industrial Emissions (kg)
Pulawy (Poland)	51–51.75	21.5–22.5	3.40e+03
Targu/Ocna Mures (Romania)	46–46.75	23.5–25	3.75e+06
Bacau (Romania)	46–47	26–27.5	3.64e+06
Slobozia (Romania)	44.25–44.75	27–28	1.48e+06
Gorlovka (Ukraine)	48.25–48.5	37.5–38.5	2.39e+06
Novomoskovsk/Shchekino (Russia)	54–54.5	37.5–38.5	2.37e+06
Togliatti (Russia)	53–53.75	49.5–50.5	5.33e+06

<sup>a</sup>The total yearly industrial emissions (kg) were obtained using SNAP 3 and 4 categories [Kuenen *et al.*, 2011] from the TNO MACC European emission inventory for the year 2007.

(e.g., nitric and sulfuric acids). In this way, secondary inorganic aerosol formation is underestimated and, consequently, NH<sub>3</sub> concentrations overestimated. On the other hand, Po Valley is considered to be a special case, which has been shown to be challenging for regional-scale models [Pernigotti *et al.*, 2013].

3. Several localized hot spots over Western Russia in 2009. These hot spots are associated with biomass burning in the end of April (23 to 30 April). IASI also observes enhanced NH<sub>3</sub> columns in that period in Eastern Russia, but the modeled plumes are smaller and more concentrated than the observed ones. This suggests not only an incorrect allocation of NH<sub>3</sub> emissions in the fire inventory but also a possible underestimation of the horizontal transport in the model (see also section 3.4).

Apart from the overall satellite model biases, a region with large model underestimation can be observed in Eastern Europe (Lithuania, Belarus, and Russia) in 2011. Satellite measurements show that large emissions are observed each year in this area in April. These are associated with forest fires [IFFN-40, 2010] and agricultural burning [e.g., Stohl *et al.*, 2007; IFFN-GFMC-16, 2011]. The year 2011 was exceptional for this area with daily NH<sub>3</sub> columns measured by IASI above 20 mg/m<sup>2</sup> from 23 to 29 April and up to 32.3 mg/m<sup>2</sup> (with an average retrieval error of 16.7%) on 28 April. Such high columns are not reproduced by the model, pointing toward missing emissions in the GFASv1.1 fire inventory.

Large model underestimates are also observed each year over several localized industrial hot spots. We have summarized these hot spots in Table 2 and marked them by black circles in the difference plots of Figure 4. The Togliatti hot spot in the Samara oblast in the Volga federal district of Russia (utmost right circle in Figure 4) is the largest of these. The large NH<sub>3</sub> concentrations in this area are likely due to the production of synthetic NH<sub>3</sub> and chemical fertilizer (see Table 2 estimates of nonagricultural emissions). The oblast is host to the world's largest NH<sub>3</sub> plants with an industrial production of 3,150,000 t NH<sub>3</sub> yr<sup>-1</sup> [International Fertilizer Development Center (IFDC), 2008]. The whole area has a leading position for this industrial production in Russia [Investsamara, 2013], this country being the third largest NH<sub>3</sub> producer in the world [International Fertilizer Development Center (IFDC), 2008; Egenhofer *et al.*, 2014]. Similar industrial hot spots can be observed in Poland, Romania, Ukraine, and Russia where lower columns in the model results are also observed every year. All these hot spot areas are known for their large NH<sub>3</sub> industrial emissions [International Fertilizer Development Center (IFDC), 2008; European Pollutant Release and Transfer Register, 2014].

The industrial discrepancies are likely explained by underestimates in the emission inventories. For the European Union-27 countries (except Romania) the yearly amount of emissions are reported by country. In Russia and Romania those are obtained using the Greenhouse gas and Air pollution INteractions and Synergies (GAINS) model [Kuenen *et al.*, 2011]. For the latter, the IASI measurements provide a first opportunity to evaluate calculated emissions based on activity data and emission factors. Note that we do not provide a quantitative amount of underestimated emissions here, as this is out of the scope of this study.

### 3.3. Intraannual Variability

In Europe, large temporal differences in NH<sub>3</sub> concentrations appear in the course of a year due to the high dependency of NH<sub>3</sub> volatilization on physical parameters (e.g., temperature and relative humidity) and local agricultural practices. Looking at the intraannual variations of the three main European NH<sub>3</sub> hot spots allows amongst other things, to assess the temporal emission profile used as input in the model. We have defined

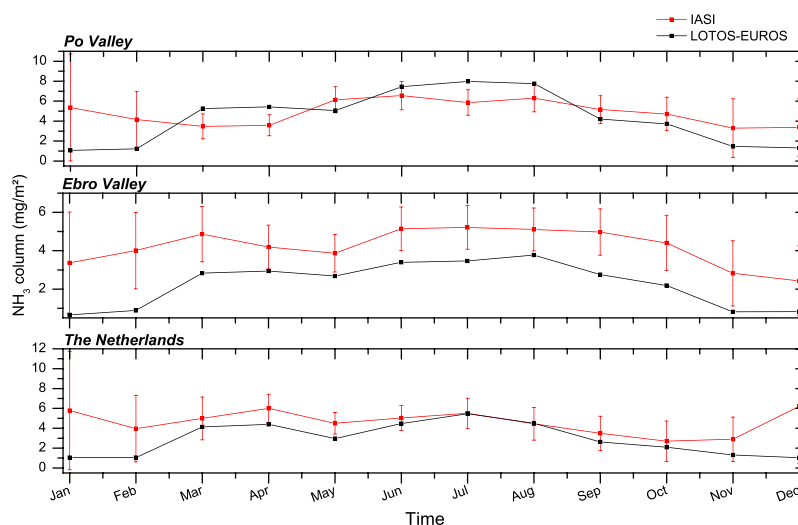


**Figure 5.**  $\text{NH}_3$  monthly composite time series ( $\text{mg}/\text{m}^2$ ) for 2008 to 2011 measured by IASI (red) and modeled by LOTOS-EUROS (black) above (top) the Po Valley, (middle) the Ebro Valley, and (bottom) the Netherlands. The error bars (red) correspond to averaged retrieval errors calculated following equation (1) around the monthly composite mean value.

three domains corresponding to  $1 \times 2^\circ$  boxes, which represent 16 grid cells of the model: the Po Valley ( $44.25\text{--}45.25^\circ\text{N}$ ,  $10\text{--}12^\circ\text{E}$ ), the Ebro Valley ( $51.25\text{--}52.25^\circ\text{N}$ ,  $4.5\text{--}6.5^\circ\text{E}$ ), and the Netherlands ( $41.25\text{--}42.25^\circ\text{N}$ ,  $0\text{--}2^\circ\text{E}$ ). Composite monthly means for the 4 years are presented in Figure 5, characterizing the seasonal cycle.

The composite time series have been derived using the observations (red) and simulations (black) from each month from each year (2008–2011). Generally, the amplitudes of the seasonal cycle in the model exceed the measured ones. One reason lies in the systematically higher measured columns in the colder months, which could be explained by the combined effect of lower emissions (see, e.g., Figure 1) and lower thermal contrasts, something which is also reflected in larger error bars. This is not the case for the warmer months, and generally, the agreement between measured and modeled average columns is better in these periods, even if systematic differences can be noted (i.e., respectively smaller and larger columns in the summer months for the Po and Ebro Valleys). The difference in amplitude is well seen for the Po Valley, where a monthly composite maximum of  $6.6 \text{ mg}/\text{m}^2$  is observed in June while a maximum of  $8.0 \text{ mg}/\text{m}^2$  is simulated by LOTOS-EUROS in July. A composite monthly minimum of  $1.1 \text{ mg}/\text{m}^2$  is simulated in January but observed in November ( $3.3 \text{ mg}/\text{m}^2$ ). The seasonal cycles are in good agreement for the Ebro Valley, but the modeled columns are in that region consistently smaller than the measured ones, possibly related to an underestimation of the emission totals in the emission inventory in this area. A misrepresentation of the diurnal emission profile for this area could also be another reason for the lower modeled columns [Pinder *et al.*, 2006]. IASI columns are the highest in July ( $5.2 \text{ mg}/\text{m}^2$ ) while the maximum simulated mean occurs in August ( $3.8 \text{ mg}/\text{m}^2$ ). The monthly minimum is observed in December ( $2.4 \text{ mg}/\text{m}^2$ ) and simulated in January ( $0.7 \text{ mg}/\text{m}^2$ ). For the Netherlands, if we exclude the winter months associated with large retrieval errors, a good agreement is found, both in the seasonality and the magnitude of the columns. A maximum of  $6.0 \text{ mg}/\text{m}^2$  is measured by IASI in April and a minimum of  $2.7 \text{ mg}/\text{m}^2$  in October. Model results present their maximum of  $5.5 \text{ mg}/\text{m}^2$  in July, while the minimum is simulated in December ( $1.0 \text{ mg}/\text{m}^2$ ). Excluding again the winter months, the comparison for the Netherlands shows the best agreement of the three sites, with both the magnitude and timing well reproduced in the model. This is expected as the fixed seasonal and diurnal emission profiles of the model have been developed based on experimental data set representative for this area [Schaap *et al.*, 2004b].

The day-to-day variability for the same three stations (same boxes as in Figure 5) is depicted in Figure 6 which shows the modeled (black,  $\text{mg}/\text{m}^2$ ) and observed (red,  $\text{mg}/\text{m}^2$ ) time series of the daily weighted mean. Note that the data coverage for the Ebro (75%) and Po Valleys (71%) in Southern Europe is higher

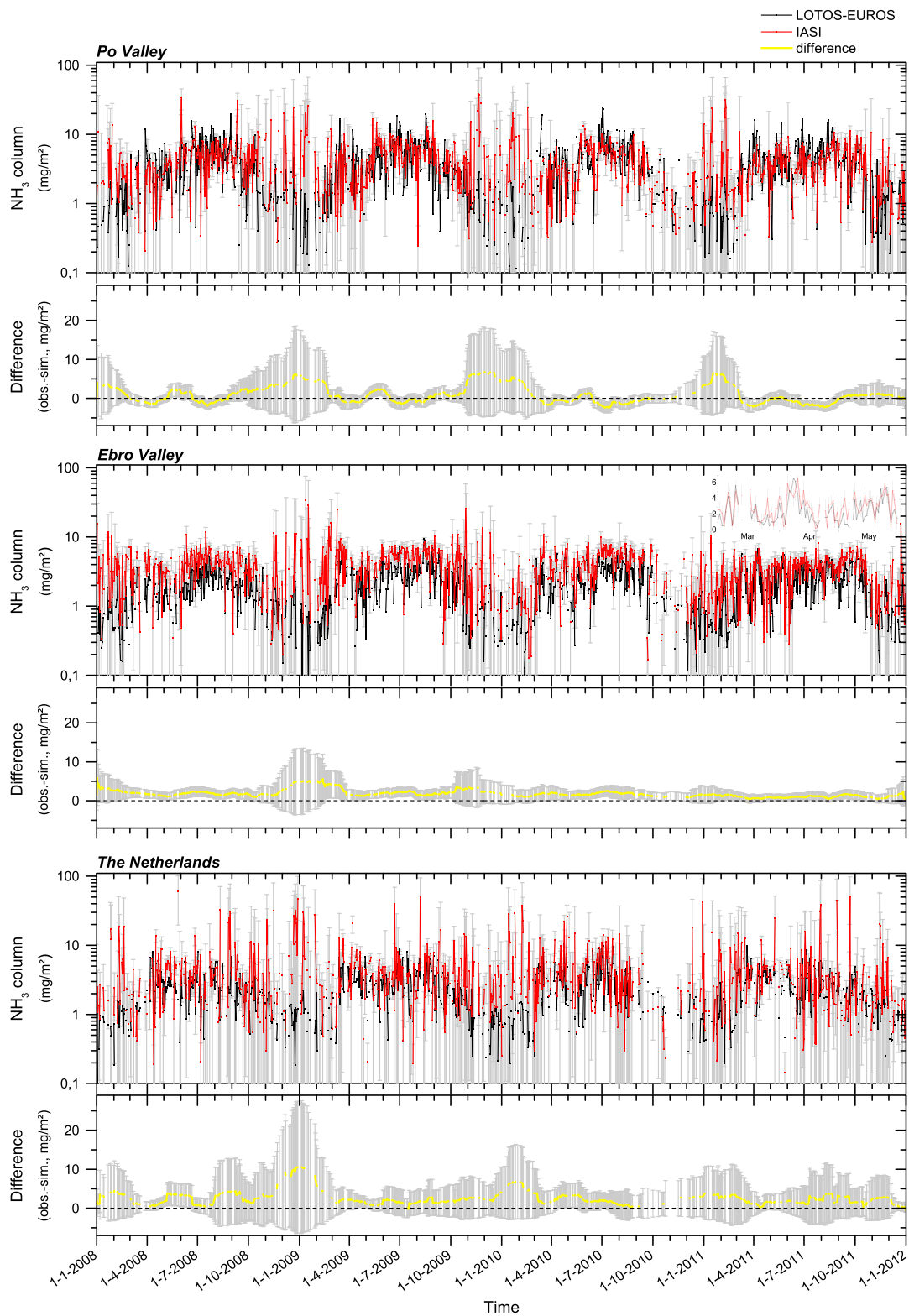


**Figure 6.** (top) Po Valley (44.25–45.25°N, 10–12°E), (middle) Ebro Valley (51.25–52.25°N, 4.5–6.5°E), and (bottom) the Netherlands (41.25–42.25°N, 0–2°E). Top panel for each station: time series of daily averaged  $\text{NH}_3$  total columns ( $\text{mg}/\text{m}^2$ , in log scale) measured by IASI (red) and modeled by LOTOS-EUROS (black) from 1 January 2008 to 31 December 2011; the error bars (grey) correspond to the error calculated using equation (1) around the daily mean value for each area. Bottom panel for each station: 30 days moving average of the difference between IASI observations and LOTOS-EUROS simulations (yellow, in  $\text{mg}/\text{m}^2$ ); the error bars (grey) correspond to a 30 days moving average of the relative errors of the daily mean applied to the difference. A zoom of March, April, and May 2011 is also provided for the Ebro Valley (see text).

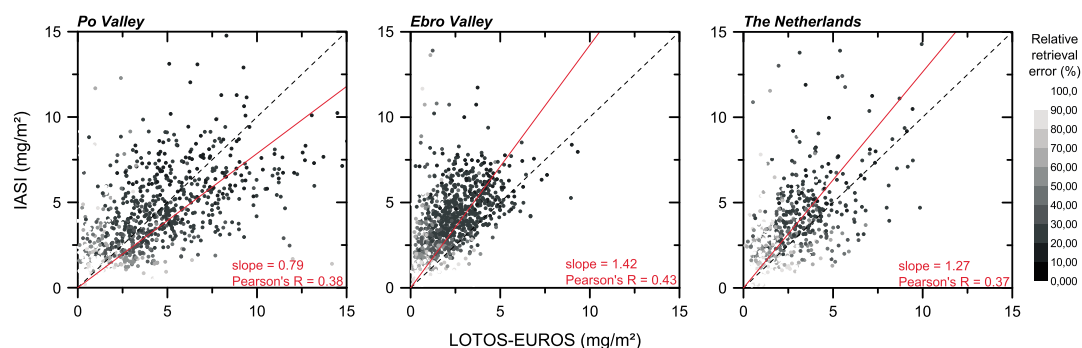


**Figure 7.** Daily comparison of the modeled  $\text{NH}_3$  total columns versus the observed ones for three regions: (left) Po Valley, (middle) Ebro Valley, and (right) Netherlands (same domains as Figures 5 and 6). Dashed lines with 1:1 ratio are indicated in black and linear regressions through the origin weighted by the IASI retrieval errors in red. The weighted regression slope and Pearson's  $R$  coefficients are also indicated in red. The color scale corresponds to the relative retrieval errors (%) of the satellite observations.

than that for the area over the Netherlands (60%) due to the difference in cloud cover. Systematic differences are observed between the modeled and observed columns with lower modeled columns for the Ebro Valley and to a lesser extent the Netherlands. Inspecting the seasonal variation shows that the wintertime measurements generally show the largest differences coinciding with large observational uncertainties. The correspondence between measured and modeled columns is best in spring/summer. However, in the running mean difference (yellow in Figure 6 (bottom)) a recurring feature is seen for the Po Valley. The modeled  $\text{NH}_3$  columns in the model simulation in June are lower than observed, whereas those in April and August are higher than the satellite data. April and August are the months with the maximum spring and summer manure application assumed in the emission profile. Hence, the signal picked up for the Po Valley may hint at a shortcoming of the seasonal variation of these profiles. As the used emission time profiles are representative for agricultural practices in Northwestern Europe (see Figure 1), they may need to be updated to reflect regional practices and cropping calendars.

On smaller time scales, daily local observed extremes are regularly reproduced. An example of this is seen in April 2011 over the Ebro Valley. On 4 April measured and modeled columns are respectively 0.8 and 0.9  $\text{mg}/\text{m}^3$ . Two days later columns reach 5  $\text{mg}/\text{m}^3$  and remain high during the following week, and after that gradually drop back to levels around 0.5  $\text{mg}/\text{m}^3$  on 20 April. For this whole episode, measured and modeled columns are consistent in magnitude and coincident in their day-to-day variability. It is worth noting that daily local maxima simulated during autumn/winter time are also observed by the satellite. It shows that observations, even when associated with large relative errors, can provide useful information on the temporal variability.

A part of the systematic differences between model and observations may be due to the constant emission behavior in each month, irrespective of the actual meteorology. Fluctuations in ambient temperature cause changes in stable emissions from one day to another 10–40% depending on the temperature difference [Skjøth *et al.*, 2011]. As the occurrence of rain out is associated with lower temperatures, a higher emission strengths during fair weather conditions may increase the  $\text{NH}_3$  lifetime and level systematically. However, potential reasons for systematic underestimation or overestimation of the observed  $\text{NH}_3$  columns could also include shortcomings in process descriptions.

With respect to the estimated error bar, in the running mean difference time series the error bar is similar in magnitude as the satellite/model difference. This can be seen not only when comparing the cold and the warmer months but also when comparing the Southern European valleys with the Netherlands. The latter has larger differences and uncertainties throughout because of less favorable thermal conditions. The retrieval error bar is therefore a realistic estimate of the uncertainty associated with the measurement. Note that in 2011 the satellite/model differences are markedly smaller than in the other years, again probably due to the improvement in the IASI temperature retrieval used as input.

Figure 7 compares the daily LOTOS-EUROS model results versus the daily IASI observations for the three hot spots in the form of scatterplots. Weighted regression lines through the origin, slopes, and weighted

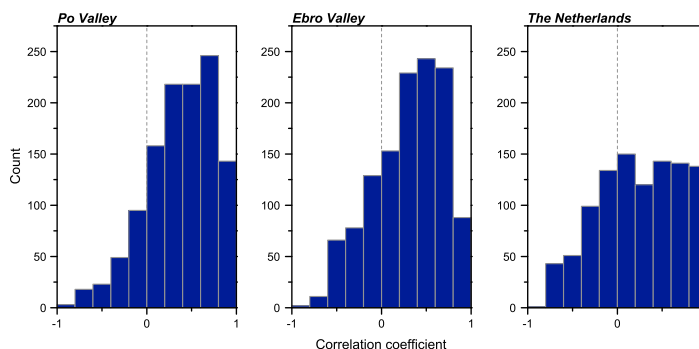


**Figure 8.** Histograms of the weighted correlation coefficient between the model and the measurement data for 11 day periods (5 days before and after each day) for the Po Valley, Ebro Valley, and Netherlands (see text for details).

Pearson correlation coefficients are indicated in red on the plots. The data points themselves are color coded according to the IASI relative retrieval error. Points far away from the regression line, in general, have a larger associated error bar, consistent with what we observed in the daily time series. The three plots are generally consistent with the picture drawn above: with modeled columns higher for the Po Valley (slope of 0.79) and lower for the Ebro Valley (slope of 1.42) and the Netherlands (slope of 1.27). Pearson's  $R$  coefficients range between 0.37 (Netherlands) and 0.43 (Ebro Valley).

What these aggregated scatterplots do not reveal is the daily dynamics of the LOTOS-EUROS model and how well it compares with the IASI retrievals. To analyze the dynamics on shorter time scales, correlation coefficients on 11 day periods (5 days before and after each day) have been calculated for the whole study period and displayed in a histogram (Figure 8) for the three sites. Only periods with at least 6 days with measurements were taken into account. Overall, for the vast majority of the periods a positive correlation is found, implying that the LOTOS-EUROS model reproduces to some extent the daily variations observed by IASI. It is best reproduced in the Po Valley, with about half of the 11 day periods being correlated with a coefficient above 0.4. It is worse for the Ebro Valley (0.35) and the Netherlands (0.25). The result for the Ebro Valley is surprising given the fact that there is a good satellite/model agreement in the seasonality for this site, but indicates that using variable daily or diurnal temporal emission profiles would be an improvement for the model. Despite the sensitivity to outliers and periods with low variability, analyzing distributions of such short-term correlation coefficients, and their response to changes in the modeling, over a multiyear period could be an efficient way to improve the temporal performance of a model.

### 3.4. Russian Fire Episode in 2010

The fire episode [Witte *et al.*, 2011; IFFN-40, 2010; Konovalov *et al.*, 2011; Krol *et al.*, 2013] which occurred during the exceptional heat wave in the summer of 2010 in European Russia released large amounts of  $\text{NH}_3$  [R'Honi *et al.*, 2013]. Table 3 depicts the estimated  $\text{NH}_3$  emissions from fires on a yearly basis over Europe, from the GFASv1.1 emission inventory. The year 2010 is confirmed by the emission inventories to be an outstanding year with 0.98 Tg of  $\text{NH}_3$  emitted by fires in the domain of study ( $-15^\circ\text{E}$  to  $55^\circ\text{E}$  and  $35^\circ\text{N}$  to  $70^\circ\text{N}$ ). This represents more than 10 times the yearly amount of the fire emission of the three other years and is equal to 13.5% of the total emitted  $\text{NH}_3$  in 2010 (from all source processes). Ninety-four percent of these 0.98 Tg were emitted in a box of  $1.5^\circ$  latitude  $\times$   $2.5^\circ$  longitude at the southeast of Moscow ( $54.5\text{--}56^\circ\text{N}$  and  $38.5\text{--}41^\circ\text{E}$ ), in good agreement with the emission range of 0.7–2.6 Tg of  $\text{NH}_3$  reported in R'Honi *et al.* [2013].

$\text{NH}_3$  distributions averaged for the fire episode (20 July to 20 August 2010) are shown in Figure 9. The LOTOS-EUROS distribution (left) is in good overall agreement with the IASI distribution (middle). Nevertheless, the distribution of the difference (observed minus modeled columns; right) reveals large discrepancies of over  $10\text{ mg/m}^2$  in and around the source area. The maximum total columns of  $\text{NH}_3$  averaged over the fire episode exceed  $123.4\text{ mg/m}^2$  (with an average retrieval error of 24%) for the satellite measurements and  $729.3\text{ mg/m}^2$  for the model results. The average distribution suggests that transport is not well accounted

**Table 3.** NH<sub>3</sub> Emitted From Fires<sup>a</sup>

	(Tg)	(% of Total)
2008	0.096	1.51
2009	0.097	1.53
2010	0.98	13.54
2011	0.076	1.20

<sup>a</sup>Yearly amount of NH<sub>3</sub> emitted from fires (left, Tg; right, % of total) over Europe (−15°E to 55°E and 35°N to 70°N) provided by the GFASv1.1 emission inventories. The total amounts were obtained using the TNO MACC European emission inventory.

for in the model, resulting in large total columns in the center of the plume, and too low columns further from the fire sources. An animation representing the evolution of the fire plume observed by IASI and modeled by LOTOS-EUROS is available in the supporting information of this paper. Both daytime and nighttime data were used for this comparison. It can be observed that the shape of the plume and the magnitude are in reasonable agreement throughout the event, with IASI again measuring consistently a more expanded plume. The animation highlights another major characteristic of this unique fire episode: the undiminished intensity of the fires during nighttime already highlighted by *Kaiser et al.* [2012] and which is a characteristic of underground peat fires.

Part of the observed model-satellite discrepancies are possibly due to the high injection heights of these specific fires for which

both the retrieval and the models are not well adapted. Forest burning in the boreal is known for sometimes large injection heights of atmospheric pollutants [Turquety et al., 2007; Sofiev et al., 2012]. Associated burning of peat land, which contains a large amount of stored organic matter, contributes to increased emissions [Turquety et al., 2007; Akagi et al., 2011]. In addition, a large umbrella-shaped pyrocumulonimbus was observed on 1 and 4 August by MODerate resolution Imaging Spectroradiometer (MODIS) and Multi-angle Imaging SpectroRadiometer (MISR) data, at an altitude of 12 km [NASA, 2013a, 2013b]. Such clouds are fire induced and can inject enormous amounts of smoke and biomass burning emissions at high altitude, up to the lower stratosphere [Fromm et al., 2010]. IASI retrievals assume a constant vertical NH<sub>3</sub> profile, which in the case of high-altitude plumes causes a measurement bias. On the other hand, the vertical extent of the LOTOS-EUROS model is limited to 3.5 km which prevents an accurate modeling of the transport and evolution of the plume.

In Figure 10, the 2010 monthly variations in NH<sub>3</sub> concentrations at Fyodorovskoe bog (Russia, NitroEurope Level-2 site, [Sutton et al., 2007; Flechard et al., 2011]) are shown as total columns from the IASI satellite (red, top panel), and as surface concentrations from the NitroEurope ground-based measurement station (blue, bottom panel). Both are compared to the results from the LOTOS-EUROS model (black, top and bottom panels). The observed peak in August is not well represented by the model, which could be explained by missing hot spots in the GFASv1.1 fire inventory, a too low emission factor for NH<sub>3</sub> from these specific fires, incorrect vertical allocation and the limited vertical extent of the model. A mean total column of 16.72 mg/m<sup>2</sup> (with an average retrieval error of 26%) in a box of 2 × 2° centered around the ground-based measurement station (56.46°N–32.92°E, white circle in Figure 9) was calculated from the IASI measurements while the LOTOS-EUROS model obtained a mean total column of 9 mg/m<sup>2</sup>. The ground-based comparison confirms the underestimations of the model: a mean surface concentration of 1.02 μg/m<sup>3</sup> is modeled for August 2010 (in the following box: 56.25–56.75°N and 32.5–33.5°E) while the ground-based station measured a mean concentration as high as 4.12 μg/m<sup>3</sup>.

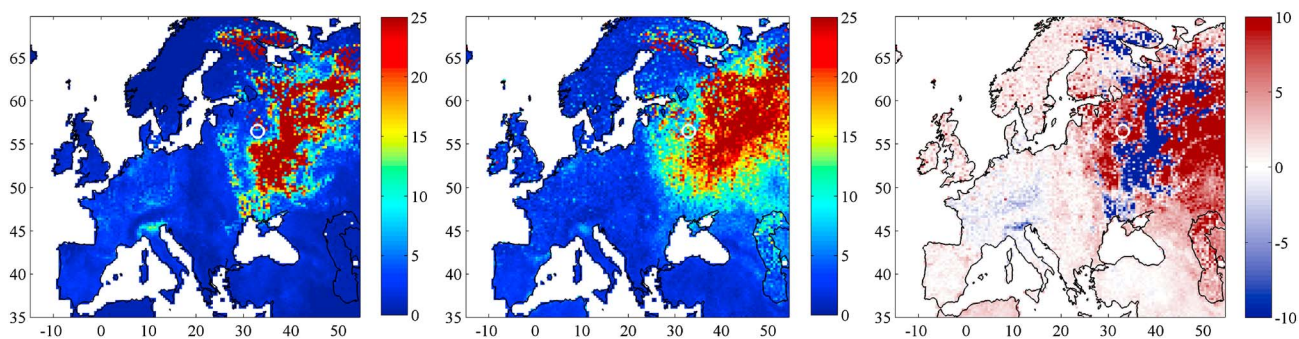


**Figure 9.** NH<sub>3</sub> distributions (left) modeled by LOTOS-EUROS (mg/m<sup>2</sup>), (middle) observed by IASI (mg/m<sup>2</sup>), and (right) the difference between both (satellite measurements minus model simulations, mg/m<sup>2</sup>) during the fire period (from 20 July to 20 August 2010) in central European Russia. The center of the white circle is the location of the ground-based measurement station of Fyodorovskoe bog providing NH<sub>3</sub> surface concentrations in Figure 10.

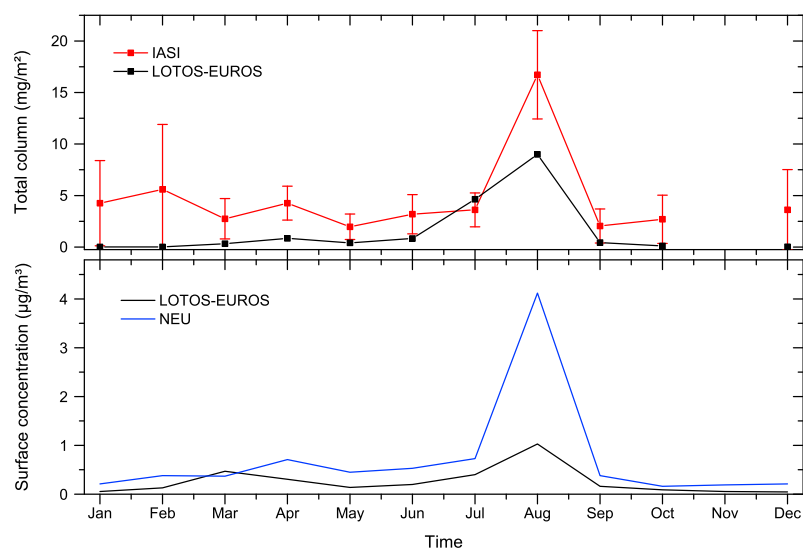


**Figure 10.** Monthly time series for 2010. (top) Monthly mean of  $\text{NH}_3$  total columns observed by IASI (red,  $\text{mg}/\text{m}^2$ ), simulated by LOTOS-EUROS (black,  $\text{mg}/\text{m}^2$ ). (bottom) Surface concentrations observed by NitroEurope station Fyodorovskoe bog (blue,  $\mu\text{g}/\text{m}^3$ ) and simulated by LOTOS-EUROS (black,  $\mu\text{g}/\text{m}^3$ ).

#### 4. Conclusions and Perspectives

Satellite observations have already been widely used to assess emission and model results of several atmospheric components. This paper introduces a novel methodology to compare unconstrained satellite retrievals of  $\text{NH}_3$  with model results, which accounts for measurement uncertainty. It allows us to present a first detailed comparison between IASI satellite observations and LOTOS-EUROS model results over Europe. Modeled and measured distributions both reveal the same agricultural source areas in Europe: the Po Valley, the Northwestern Europe, and the Ebro Valley. A good overall agreement is observed on the mean distributions, also over remote areas and over sea when transport is observed. In general, modeled simulations are slightly lower than the measured ones. However, a decrease in this bias has been identified from 2008 ( $1.92 \text{ mg}/\text{m}^2$ ) to 2011 ( $1.4$ ) which could be due to improvements of the retrieval input L2 data. The Po Valley and Brittany are the only areas where the model shows higher columns each year.

The largest differences in the mean distributions are observed over several industrial areas in Eastern Europe and Russia and are likely linked to the production of synthetic fertilizers. This is especially apparent over Samara oblast in Russia, host to the largest synthetic  $\text{NH}_3$  producer in the world. It is the first time that industrial  $\text{NH}_3$  is observed so clearly, suggesting, although a quantitative estimation was not obtained, strong underestimation of emissions in the inventories. These unexpected differences constitute a clear example of the added value of IASI satellite measurements. A lot of effort is devoted to characterizing  $\text{NH}_3$  emissions from agriculture and biomass burning; our results emphasize the need for similar efforts for industrial emissions. For instance, current regulations on  $\text{NO}_x$  emissions have led to the widespread use of  $\text{NH}_3$  reduction systems to convert them to  $\text{N}_2$  [Radojevic, 1998]; the excess  $\text{NH}_3$ , referred to as the  $\text{NH}_3$  slip is difficult to monitor [Staudt, 2000]. A next step could be to explore if more quantitative emission evaluation of point sources is possible following novel approaches as developed for  $\text{SO}_2$  [McLinden et al., 2014].

Large differences are also observed for the fires in Eastern Europe and Western Russia in spring 2009 and 2011 and the summer of 2010, pointing to imperfections in the GFASv1.1 emission inventories for this region and/or limitations in the modeling of biomass burning events. It is evident that there are problems in the allocation of the fire emissions and the subsequent horizontal transport in the modeling seems to be underestimated, which leads to smaller and more concentrated modeled plumes. This was especially apparent in the study of the 2010 Russian fires and was confirmed by a comparison with ground-based observations outside the burning area. It should be emphasized that this event presents a challenge for the CTMs, for the meteorological model as well as for the satellite retrievals. For IASI, the assumed vertical profiles introduce a bias in the retrieved columns. For the LOTOS-EUROS model, its vertical extent of 3.5 km is a limitation for

modeling the high-altitude plumes. Currently, a new LOTOS-EUROS model version with an extended vertical structure is being developed, such that a better comparison with the IASI satellite in such extreme events will be possible in the future. It is also worth noting that vertical distribution is very variable among fire emission products and under close scrutiny of other groups [see, for example, Sofiev *et al.*, 2012; Menut *et al.*, 2013; Turquety *et al.*, 2014].

To assess the temporal performance of the model and measurements, a detailed comparison was carried out over three agricultural hot spot areas. Composite monthly means reveal that the seasonality measured by IASI is well captured by the LOTOS-EUROS model. Differences are largest during the coldest months but consistent with the larger uncertainty estimates during these periods. The best agreement is found over the Netherlands, both in terms of magnitude and timing, most likely as the fixed timing of the emissions was determined from experimental data sets from this country. In terms of magnitude, the largest differences are observed over the Ebro Valley, where LOTOS-EUROS columns are consistently lower in comparison with IASI ones, possibly due to underestimated emissions and/or a misrepresentation of the diurnal emission profile. For the Po Valley, a characteristic feature is recurring in the satellite/model difference every year and is likely caused by incorrect timing of the emissions. The distinct seasonal patterns of these three sites, underline the need for improved timing of emissions.

Moving to the daily mean time series, measured and modeled columns are consistent in magnitude and their day-to-day variability when measurement uncertainty is taken into account. From the daily analysis of the satellite/model differences, it is apparent that the estimated uncertainty is overall a good measure of the retrieval error. Also, the daily dynamics of the model are in reasonable agreement with the measurements, as evident from the analysis of short-term correlation coefficients of 11 day periods. Tracking changes in the distribution of correlation coefficients could be an efficient way for evaluating potential improvements in the day-to-day variability of the model. We aim to evaluate the incorporation of dynamic emission modules [Skjoth *et al.*, 2011; Hamaoui-Laguel *et al.*, 2014] using IASI data when modules representative for Europe become available.

Note that an analogous model/satellite analysis for the nighttime as the one presented here could be made. Even though retrieval uncertainties are generally larger, in favorable nighttime conditions sensitivity to NH<sub>3</sub> can be as good as for daytime measurements. This is the case when NH<sub>3</sub> columns are very large, as for instance observed above biomass burning events (see section 3.4 and supporting information). Another example of enhanced nighttime sensitivity occurs when inversion layers amplify the thermal contrast [Bauduin *et al.*, 2014; Boynard *et al.*, 2014]. Moreover, we observe that in wintertime, daily temporal variations are nicely captured by the IASI measurements. This shows that despite larger errors, winter and nighttime measurements can provide useful information and should be exploited in the future.

As a final conclusion, this study has shown that IASI provides unprecedented data under clear sky, which can be used to investigate the dependency of NH<sub>3</sub> emissions on localized agricultural practices and on parameters driving the volatilization. IASI-NH<sub>3</sub> data also provide information where to improve emission inventories and the development of temporal profiles specific to each part of the European domain. The results, over a region where IASI retrievals are complex because of unfavorable temperature conditions but where models are efficient and reliable, demonstrate the potential of satellites measurements to improve NH<sub>3</sub> monitoring in the rest of the world. From a satellite retrieval perspective, the comparison with LOTOS-EUROS also indicates that the NH<sub>3</sub> retrieval algorithm is robust. However, a thorough validation would be useful to better quantify possible biases and uncertainties in the satellite retrievals prior to using this data in assimilation systems. A specific measurement campaign is currently in progress in the Netherlands (Cabauw site) using a set of complementary instruments.

## References

- Adams, P. J., N. M. Donahue, and S. N. Pandis (2013), Atmospheric nanoparticles and climate change, *AtChE J.*, 59(11), 4006–4019, doi:10.1002/aic.14242.
- Akagi, S. K., R. J. Yokelson, C. Wiedinmyer, M. J. Alvarado, J. S. Reid, T. Karl, J. D. Crouse, and P. O. Wennberg (2011), Emission factors for open and domestic biomass burning for use in atmospheric models, *Atmos. Chem. Phys.*, 11(9), 4039–4072, doi:10.5194/acp-11-4039-2011.
- Andela, N., J. Kaiser, A. Heil, T. van Leeuwen, G. van der Werf, M. Wooster, S. Remy, and M. Schultz (2013), Assessment of the Global Fire Assimilation System (GFASv1), *MACC-II Deliverable Report D\_31.2*, MACC-II project, ECMWF, Reading, U. K.

## Acknowledgments

The IASI-NH<sub>3</sub> observations are available on request at ULB. IASI has been developed and built under the responsibility of the "Centre National d'Etudes Spatiales" (CNES, France). It is flown on board the Metop satellites as part of the EUMETSAT Polar System. The IASI L1 data are received through the EUMETCast near real-time data distribution service. The LOTOS-EUROS model results are available on request at TNO. The ground-based measurements used for the comparison in Russia (2010) were collected within the framework of the "NitroEurope IP" project 017841. We are grateful to all scientists involved in this project who made this data set available, especially Andrej Varlagin and Chris Flechard. The research in Belgium was funded by the F.R.S.-FNRS, the Belgian State Federal Office for Scientific, Technical and Cultural Affairs. M. Van Damme is grateful to the "Fonds pour la Formation à la Recherche dans l'Industrie et dans l'Agriculture" of Belgium for a Ph.D. grant (Boursier FRIA). L. Clarisse and P.-F. Coheur are respectively Postdoctoral Researcher and Research Associate (Chercheur Qualifié) with F.R.S.-FNRS. C. Clerbaux is grateful to CNES for scientific collaboration and financial support. We gratefully acknowledge the support from the project "Effects of Climate Change on Air Pollution Impacts and Response Strategies for European Ecosystems" (ÉCLAIRE), funded under the EC Seventh Framework Programme (grant agreement 282910), as well as the support from the "Netherlands Organization for Scientific Research" (NWO). We also would like to thank J. Hadji-Lazarou, R. Kranenburg, J. Kuenen, Y. Ngadi, and A. Segers for their assistance.

- August, T., D. Klaes, P. Schlüssel, T. Hultberg, M. Crapeau, A. Arriaga, A. O'Carroll, D. Coppens, R. Munro, and X. Calbet (2012), IASI on Metop-A: Operational Level 2 retrievals after five years in orbit, *J. Quant. Spectrosc. Radiat. Transfer*, *113*(11), 1340–1371, doi:10.1016/j.jqsrt.2012.02.028.
- Banzhaf, S., M. Schaap, A. Kerschbaumer, E. Reimer, R. Stern, E. van der Swaluw, and P. Bultjes (2012), Implementation and evaluation of pH-dependent cloud chemistry and wet deposition in the chemical transport model REM-Calgrid, *Atmos. Environ.*, *49*, 378–390, doi:10.1016/j.atmosenv.2011.10.069.
- Barriopedro, D., E. M. Fischer, J. Luterbacher, R. M. Trigo, and R. Garcia-Herrera (2011), The hot summer of 2010: Redrawing the temperature record map of Europe, *Science*, *332*(6026), 220–224, doi:10.1126/science.1201224.
- Bauduin, S., L. Clarisse, C. Clerbaux, D. Hurtmans, and P.-F. Coheur (2014), IASI observations of sulfur dioxide (SO<sub>2</sub>) in the boundary layer of Norilsk, *J. Geophys. Res. Atmos.*, *119*, 4253–4263, doi:10.1002/2013JD021405.
- Beer, R., et al. (2008), First satellite observations of lower tropospheric ammonia and methanol, *Geophys. Res. Lett.*, *35*, L09801, doi:10.1029/2008GL033642.
- Bessagnet, B., A. Colette, P. Thunis, and L. Rouil (2013), Eurodelta3—Status and link with HTAP, presentation at the TF HTAP meeting held in December in San Francisco, USA. [Available at [http://htap.org/meetings/2013/2013\\_12/Thurs/Collette%20EuroDelta.pdf](http://htap.org/meetings/2013/2013_12/Thurs/Collette%20EuroDelta.pdf) (last access: 12 June 2014)].
- Bouwman, A. F., L. J. M. Boumans, and N. H. Batjes (2002), Estimation of global NH<sub>3</sub> volatilization loss from synthetic fertilizers and animal manure applied to arable lands and grasslands, *Global Biogeochem. Cycles*, *16*(2), 1024, doi:10.1029/2000GB001389.
- Boynard, A., et al. (2014), First simultaneous space measurements of atmospheric pollutants in the boundary layer from IASI: A case study in the North China Plain, *Geophys. Res. Lett.*, *41*(2), 645–651, doi:10.1002/2013GL058333.
- Clarisse, L., C. Clerbaux, F. Dentener, D. Hurtmans, and P.-F. Coheur (2009), Global ammonia distribution derived from infrared satellite observations, *Nat. Geosci.*, *2*(7), 479–483, doi:10.1038/ngeo551.
- Clarisse, L., M. Shephard, F. Dentener, D. Hurtmans, K. Cady-Pereira, F. Karagulian, M. Van Damme, C. Clerbaux, and P.-F. Coheur (2010), Satellite monitoring of ammonia: A case study of the San Joaquin Valley, *J. Geophys. Res.*, *115*, D13302, doi:10.1029/2009JD013291.
- Clerbaux, C., et al. (2009), Monitoring of atmospheric composition using the thermal infrared IASI/MetOp sounder, *Atmos. Chem. Phys.*, *9*(16), 6041–6054, doi:10.5194/acp-9-6041-2009.
- Coheur, P.-F., L. Clarisse, S. Turquety, D. Hurtmans, and C. Clerbaux (2009), IASI measurements of reactive trace species in biomass burning plumes, *Atmos. Chem. Phys.*, *9*(15), 5655–5667, doi:10.5194/acp-9-5655-2009.
- Denier van der Gon, H., A. Visschedijk, H. Van der Brugh, and R. Dröge (2010), A high resolution European emission data base for the year 2005. A contribution to UBA-Projekt PAREST: Particle Reduction Strategies, *TNO Rep. TNO-034-UT-2010-01895\_RPT-ML*, TNO, Utrecht, Netherlands.
- Denier van der Gon, H., C. Hendriks, J. Kuenen, A. Segers, and A. Visschedijk (2011), Description of current temporal emission patterns and sensitivity of predicted AQ for temporal emission patterns, *EU FP7 MACC Deliverable Rep. D\_D-EMIS\_1.3*, TNO, Utrecht, Netherlands.
- Dufour, G., M. Eremenko, A. Griesfeller, B. Barret, E. LeFlochmoën, C. Clerbaux, J. Hadji-Lazaro, P.-F. Coheur, and D. Hurtmans (2012), Validation of three different scientific ozone products retrieved from IASI spectra using ozonesondes, *Atmos. Meas. Tech.*, *5*(3), 611–630, doi:10.5194/amt-5-611-2012.
- EEA-European Environment Agency (2012), Ammonia (NH<sub>3</sub> emissions (APE 003))—Assessment published December 2012. [Available at <http://www.eea.europa.eu/data-and-maps/indicators/eea-32-ammonia-nh3-emissions-1/assessment-2> (last access: 20 August 2013).]
- Egenhofer, C., L. Schrefler, V. Rizo, F. Infelise, G. Luchetta, F. Simonelli, W. Stoefs, J. Timini, and L. Colantoni (2014), Composition and drivers of energy prices and costs in energy intensive industries: The case of the chemical industry—Ammonia, *Tech. Rep.*, Center for European Policy Studies, Brussels, Belgium.
- Emission Database for Global Atmospheric Research (2011), Source: EC-JRC/PBL. EDGAR version 4.2. [Available at <http://edgar.jrc.ec.europa.eu> (last access: 15th October 2012).]
- Erisman, J. W., and M. Schaap (2004), The need for ammonia abatement with respect to secondary PM reductions in Europe, *Environ. Pollut.*, *129*(1), 159–163, doi:10.1016/j.envpol.2003.08.042.
- Erisman, J. W., A. Bleeker, J. Galloway, and M. Sutton (2007), Reduced nitrogen in ecology and the environment, *Environ. Pollut.*, *150*(1), 140–149, doi:10.1016/j.envpol.2007.06.033.
- Erisman, J. W., M. A. Sutton, J. Galloway, Z. Klimont, and W. Winiwarter (2008), How a century of ammonia synthesis changed the world, *Nat. Geosci.*, *1*(10), 636–639, doi:10.1038/ngeo325.
- Erisman, J. W., J. N. Galloway, S. Seitzinger, A. Bleeker, N. B. Dise, A. M. R. Petrescu, A. M. Leach, and W. de Vries (2013), Consequences of human modification of the global nitrogen cycle, *Philos. Trans. R. Soc. London, Ser. B*, *368*(1621), 20130116, doi:10.1098/rstb.2013.0116.
- European Pollutant Release and Transfer Register (2014), Pollutant releases. [Available at <http://prtr.ec.europa.eu/> (last access: 25 March 2014).]
- Flechard, C. R., et al. (2011), Dry deposition of reactive nitrogen to European ecosystems: A comparison of inferential models across the NitroEurope network, *Atmos. Chem. Phys.*, *11*(6), 2703–2728, doi:10.5194/acp-11-2703-2011.
- Flechard, C. R., R.-S. Massad, B. Loubet, E. Personne, D. Simpson, J. O. Bash, E. J. Cooter, E. Nemitz, and M. A. Sutton (2013), Advances in understanding, models and parameterizations of biosphere-atmosphere ammonia exchange, *Biogeosciences*, *10*(7), 5183–5225, doi:10.5194/bg-10-5183-2013.
- Fountoukis, C., and A. Nenes (2007), ISORROPIA II: A computationally efficient thermodynamic equilibrium model for K<sup>+</sup>-Ca<sup>2+</sup>-Mg<sup>2+</sup>-NH<sub>4</sub><sup>+</sup>-Na<sup>+</sup>-SO<sub>4</sub><sup>2-</sup>-NO<sub>3</sub><sup>-</sup>-Cl<sup>-</sup>-H<sub>2</sub>O aerosols, *Atmos. Chem. Phys.*, *7*(17), 4639–4659, doi:10.5194/acp-7-4639-2007.
- Fowler, D., et al. (2013), The global nitrogen cycle in the twenty-first century, *Philos. Trans. R. Soc. London, Ser. B*, *368*(1621), 20130164, doi:10.1098/rstb.2013.0164.
- Fromm, M., D. T. Lindsey, R. Servranckx, G. Yue, T. Trickl, R. Sica, P. Doucet, and S. Godin-Beekmann (2010), The untold story of pyrocumulonimbus, *Bull. Am. Meteorol. Soc.*, *91*(9), 1193–1209, doi:10.1175/2010BAMS3004.1.
- Ginoux, P., L. Clarisse, C. Clerbaux, P.-F. Coheur, O. Dubovik, N. C. Hsu, and M. Van Damme (2012), Mixing of dust and NH<sub>3</sub> observed globally over anthropogenic dust sources, *Atmos. Chem. Phys.*, *12*(16), 7351–7363, doi:10.5194/acp-12-7351-2012.
- Gong, L., et al. (2013), Role of atmospheric ammonia in particulate matter formation in Houston during summertime, *Atmos. Environ.*, *77*, 893–900, doi:10.1016/j.atmosenv.2013.04.079.
- Hamaoui-Laguel, L., F. Meleux, M. Beekmann, B. Bessagnet, S. Générumont, P. Cellier, and L. Létinois (2014), Improving ammonia emissions in air quality modelling for France, *Atmos. Environ.*, *92*, 584–595, doi:10.1016/j.atmosenv.2012.08.002.
- Heald, C. L., et al. (2012), Atmospheric ammonia and particulate inorganic nitrogen over the United States, *Atmos. Chem. Phys.*, *12*(21), 10,295–10,312, doi:10.5194/acp-12-10295-2012.

- Hertel, O., et al. (2012), Governing processes for reactive nitrogen compounds in the European atmosphere, *Biogeosciences*, 9(12), 4921–4954, doi:10.5194/bg-9-4921-2012.
- Hilton, F., et al. (2012), Hyperspectral Earth observation from IASI: Five years of accomplishments, *Bull. Am. Meteorol. Soc.*, 93, 347–370, doi:10.1175/BAMS-D-11-00027.1.
- Hutchings, N., S. Sommer, J. Andersen, and W. Asman (2001), A detailed ammonia emission inventory for Denmark, *Atmos. Environ.*, 35(11), 1959–1968, doi:10.1016/S1352-2310(00)00542-2.
- IFFN-40 (2010), International Forest Fires News. [Available at <http://www.fire.uni-freiburg.de/iffn/iffn.htm> (last access: 25 March 2014).]
- IFFN-GFMC-16 (2011), Global Fire Monitoring Center, Global Wildland Fire Network Bulletin No. 16. [Available at <http://www.fire.uni-freiburg.de/GFMCnew/2011/GFMC-Bulletin-02-2011.pdf> (last access: 11 April 2014).]
- International Fertilizer Development Center (IFDC) (2008), Worldwide ammonia capacity listing by plant, *Tech. Rep.*, An International Center for Soil Fertility and Agricultural Development, Muscle Shoals, Alabama.
- Investsamara (2013), Samara as a major scientific and industrial center. [Available at [http://investsamara.ru/en/samara\\_region/center/](http://investsamara.ru/en/samara_region/center/) (last access: 20 August 2013).]
- Kaiser, J. W., et al. (2012), Biomass burning emissions estimated with a global fire assimilation system based on observed fire radiative power, *Biogeosciences*, 9(1), 527–554, doi:10.5194/bg-9-527-2012.
- Kharol, S. K., R. V. Martin, S. Philip, S. Vogel, D. K. Henze, D. Chen, Y. Wang, Q. Zhang, and C. L. Heald (2013), Persistent sensitivity of Asian aerosol to emissions of nitrogen oxides, *Geophys. Res. Lett.*, 40(5), 1021–1026, doi:10.1002/grl.50234.
- Konovalov, I. B., M. Beekmann, I. N. Kuznetsova, A. Yurova, and A. M. Zvyagintsev (2011), Atmospheric impacts of the 2010 Russian wildfires: Integrating modelling and measurements of an extreme air pollution episode in the Moscow region, *Atmos. Chem. Phys.*, 11(19), 10,031–10,056, doi:10.5194/acp-11-10031-2011.
- Krol, M., et al. (2013), How much CO was emitted by the 2010 fires around Moscow?, *Atmos. Chem. Phys.*, 13(9), 4737–4747, doi:10.5194/acp-13-4737-2013.
- Kuenen, J., H. Denier van der Gon, A. Visschedijk, H. van der Brugh, and R. van Gijlswijk (2011), MACC European emission inventory for the years 2003–2007, *TNO Rep. TNO-060-UT-2011-00588*, TNO, Utrecht, Netherlands.
- McLinden, C. A., V. Fioletov, K. F. Boersma, S. K. Kharol, N. Krotkov, L. Lamsal, P. A. Makar, R. V. Martin, J. P. Veefkind, and K. Yang (2014), Improved satellite retrievals of NO<sub>2</sub> and SO<sub>2</sub> over the Canadian oil sands and comparisons with surface measurements, *Atmos. Chem. Phys.*, 14(7), 3637–3656, doi:10.5194/acp-14-3637-2014.
- Menut, L., et al. (2013), CHIMERE 2013: A model for regional atmospheric composition modelling, *Geosci. Model Dev.*, 6(4), 981–1028, doi:10.5194/gmd-6-981-2013.
- NASA (2013a), Russian firestorm: Finding a fire cloud from space. [Available at <http://earthobservatory.nasa.gov/Features/PyroClouds/> (last access: 20 August 2013).]
- NASA (2013b), Fires and smoke in Russia. [Available at <http://earthobservatory.nasa.gov/IOTD/view.php?id=45046> (last access: 20 August 2013).]
- Nowak, J. B., J. A. Neuman, R. Bahreini, A. M. Middlebrook, J. S. Holloway, S. A. McKeen, D. D. Parrish, T. B. Ryerson, and M. Trainer (2012), Ammonia sources in the California South Coast Air Basin and their impact on ammonium nitrate formation, *Geophys. Res. Lett.*, 39, L07804, doi:10.1029/2012GL051197.
- Paulot, F., and D. J. Jacob (2014), Hidden cost of U.S. agricultural exports: Particulate matter from ammonia emissions, *Environ. Sci. Technol.*, 48(2), 903–908, doi:10.1021/es4034793.
- Pernigotti, D., et al. (2013), POMI: A model inter-comparison exercise over the Po Valley, *Air Qual. Atmos. Health*, 6(4), 701–715, doi:10.1007/s11869-013-0211-1.
- Pinder, R. W., P. J. Adams, S. N. Pandis, and A. B. Gilliland (2006), Temporally resolved ammonia emission inventories: Current estimates, evaluation tools, and measurement needs, *J. Geophys. Res.*, 111, D16310, doi:10.1029/2005JD006603.
- Pinder, R. W., J. T. Walker, J. O. Bash, K. E. Cady-Pereira, D. K. Henze, M. Luo, G. B. Osterman, and M. W. Shephard (2011), Quantifying spatial and seasonal variability in atmospheric ammonia with in situ and space-based observations, *Geophys. Res. Lett.*, 38, L04802, doi:10.1029/2010GL046146.
- Pope III, C. A., M. Ezzati, and D. W. Dockery (2009), Fine-particulate air pollution and life expectancy in the United States, *N. Engl. J. Med.*, 360(4), 376–386, doi:10.1056/NEJMs0805646.
- Poullot, G., T. Pierce, H. Denier van der Gon, M. Schaap, M. Moran, and U. Nopmongcol (2012), Comparing emission inventories and model-ready emission datasets between Europe and North America for the AQMEII project, *Atmos. Environ.*, 53, 4–14, doi:10.1016/j.atmosenv.2011.12.041.
- Radojevic, M. (1998), Reduction of nitrogen oxides in flue gases, *Environ. Pollut.*, 102(1), 685–689, doi:10.1016/S0269-7491(98)80099-7.
- Reis, S., R. W. Pinder, M. Zhang, G. Lijie, and M. A. Sutton (2009), Reactive nitrogen in atmospheric emission inventories, *Atmos. Chem. Phys.*, 9(19), 7657–7677, doi:10.5194/acp-9-7657-2009.
- R'Honi, Y., L. Clarisse, C. Clerbaux, D. Hurtmans, V. Duflot, S. Turquety, Y. Ngadi, and P.-F. Coheur (2013), Exceptional emissions of NH<sub>3</sub> and HCOOH in the 2010 Russian wildfires, *Atmos. Chem. Phys.*, 13(8), 4171–4181, doi:10.5194/acp-13-4171-2013.
- Rodgers, C. (2000), *Inverse Methods for Atmospheric Sounding: Theory and Practice*, World Scientific Press, Singapore, doi:10.1142/9789812813718.
- Schaap, M., H. A. C. Denier Van Der Gon, F. J. Dentener, A. J. H. Visschedijk, M. Van Loon, H. M. ten Brink, J.-P. Putaud, B. Guillaume, C. Lioussé, and P. J. H. Buitjes (2004a), Anthropogenic black carbon and fine aerosol distribution over Europe, *J. Geophys. Res.*, 109, D18207, doi:10.1029/2003JD004330.
- Schaap, M., M. van Loon, H. M. ten Brink, F. J. Dentener, and P. J. H. Buitjes (2004b), Secondary inorganic aerosol simulations for Europe with special attention to nitrate, *Atmos. Chem. Phys.*, 4(3), 857–874, doi:10.5194/acp-4-857-2004.
- Schaap, M., R. Timmermans, M. Roemer, G. Boersen, P. Buitjes, F. Sauter, G. Velders, and J. Beck (2008), The LOTOS-EUROS model: Description, validation and latest developments, *Int. J. Environ. Pollut.*, 32, 270–290, doi:10.1504/IJEP.2008.017106.
- Schiferl, L. D., C. L. Heald, J. B. Nowak, J. S. Holloway, J. A. Neuman, R. Bahreini, I. B. Pollack, T. B. Ryerson, C. Wiedinmyer, and J. G. Murphy (2014), An investigation of ammonia and inorganic particulate matter in California during the CalNex campaign, *J. Geophys. Res.*, 119, 1883–1902, doi:10.1002/2013JD020765.
- Shephard, M. W., et al. (2011), TES ammonia retrieval strategy and global observations of the spatial and seasonal variability of ammonia, *Atmos. Chem. Phys.*, 11(20), 10,743–10,763, doi:10.5194/acp-11-10743-2011.
- Simpson, D., H. Fagerli, J. Jonson, S. Tsyro, P. Wind, and J.-P. Tuovinen (2003), Transboundary acidification, eutrophication and ground level ozone in Europe. Part 1. Unified EMEP model description, *EMEP/MSC-W Report EMEP Report 1/2003*, Norwegian Meteorological Institute, Oslo, Norway. ISSN 0806–4520.

- Skj oth, C. A., et al. (2011), Spatial and temporal variations in ammonia emissions—A freely accessible model code for Europe, *Atmos. Chem. Phys.*, *11*(11), 5221–5236, doi:10.5194/acp-11-5221-2011.
- Sofiev, M., T. Ermakova, and R. Vankevich (2012), Evaluation of the smoke-injection height from wild-land fires using remote-sensing data, *Atmos. Chem. Phys.*, *12*(4), 1995–2006, doi:10.5194/acp-12-1995-2012.
- Staudt, J. E. (2000), Measuring ammonia slip from post combustion NO<sub>x</sub> reduction systems, *Tech. Rep.*, Andover Technology Partners, North Andover, Massachusetts. ICAC Forum 2000.
- Stohl, A., et al. (2007), Arctic smoke—Record high air pollution levels in the European Arctic due to agricultural fires in Eastern Europe in spring 2006, *Atmos. Chem. Phys.*, *7*(2), 511–534, doi:10.5194/acp-7-511-2007.
- Streets, D. G., et al. (2013), Emissions estimation from satellite retrievals: A review of current capability, *Atmos. Environ.*, *77*, 1011–1042, doi:10.1016/j.atmosenv.2013.05.051.
- Sutton, M., et al. (2007), Challenges in quantifying biosphere-atmosphere exchange of nitrogen species, *Environ. Pollut.*, *150*(1), 125–139, doi:10.1016/j.envpol.2007.04.014.
- Sutton, M. A., et al. (2013), Towards a climate-dependent paradigm of ammonia emission and deposition, *Philos. Trans. R. Soc. London, Ser. B*, *368*(1621), 20130166, doi:10.1098/rstb.2013.0166.
- Turquet, S., et al. (2007), Inventory of boreal fire emissions for North America in 2004: Importance of peat burning and pyroconvective injection, *J. Geophys. Res.*, *112*, D12503, doi:10.1029/2006JD007281.
- Turquet, S., L. Menut, B. Bessagnet, A. Anav, N. Viovy, F. Maignan, and M. Wooster (2014), APIFLAME v1.0: High-resolution fire emission model and application to the Euro-Mediterranean region, *Geosci. Model Dev.*, *7*(2), 587–612, doi:10.5194/gmd-7-587-2014.
- Van Damme, M., L. Clarisse, C. L. Heald, D. Hurtmans, Y. Ngadi, C. Clerbaux, A. J. Dolman, J. W. Erisman, and P. F. Coheur (2014), Global distributions, time series and error characterization of atmospheric ammonia (NH<sub>3</sub>) from IASI satellite observations, *Atmos. Chem. Phys.*, *14*(6), 2905–2922, doi:10.5194/acp-14-2905-2014.
- van Pul, A., O. Hertel, C. Geels, A. Dore, M. Vieno, H. Jaarsveld, R. Bergstr om, M. Schaap, and H. Fagerli (2009), Modelling of the atmospheric transport and deposition of ammonia at a national and regional scale, in *Atmospheric Ammonia*, edited by A. van Pul et al., pp. 301–358, Springer, Netherlands, doi:10.1007/978-1-4020-9121-6\_19.
- van Zanten, M. C., F. J. Sauter, R. J. Wichink Kruit, J. A. van Jaarsveld, and M. A. J. van Pul (2010), Description of the DEPAC module: Dry deposition modelling with DEPAC\_GCN2010, *Rivm Report 680180001/2010*, RIVM, Bilthoven, Netherlands.
- Velthof, G., C. van Bruggen, C. Groenestein, B. de Haan, M. Hoogeveen, and J. Huijsmans (2012), A model for inventory of ammonia emissions from agriculture in the Netherlands, *Atmos. Environ.*, *46*, 248–255, doi:10.1016/j.atmosenv.2011.09.075.
- von Bobruzki, K., et al. (2010), Field inter-comparison of eleven atmospheric ammonia measurement techniques, *Atmos. Meas. Tech.*, *3*(1), 91–112, doi:10.5194/amt-3-91-2010.
- Walker, J. M., S. Philip, R. V. Martin, and J. H. Seinfeld (2012), Simulation of nitrate, sulfate, and ammonium aerosols over the United States, *Atmos. Chem. Phys.*, *12*(22), 11,213–11,227, doi:10.5194/acp-12-11213-2012.
- Wichink Kruit, R. J., W. van Pul, F. Sauter, M. van den Broek, E. Nemitz, M. Sutton, M. Krol, and A. Holtslag (2010), Modeling the surface-atmosphere exchange of ammonia, *Atmos. Environ.*, *44*(7), 945–957, doi:10.1016/j.atmosenv.2009.11.049.
- Wichink Kruit, R. J., M. Schaap, F. J. Sauter, M. C. van Zanten, and W. A. J. van Pul (2012a), Modeling the distribution of ammonia across Europe including bi-directional surface-atmosphere exchange, *Biogeosciences*, *9*(12), 5261–5277, doi:10.5194/bg-9-5261-2012.
- Wichink Kruit, R., M. Schaap, F. Sauter, E. van der Waluw, and E. Weijers (2012b), Improving the understanding of the secondary inorganic aerosol distribution over the Netherlands, *TNO Rep. TNO-060-UT-2012-00334*, TNO, Utrecht, Netherlands.
- Wichink Kruit, R. J., et al. (2013), ECLAIRE model inter-comparison of atmospheric nitrogen deposition and concentrations over Europe, presentation at the ACCENT-Plus Symposium held in September in Urbino, Italy. [Available at <http://www.accent-network.org/symposium2013/docs/presentations/18sept/7-20130918%20Wichink%20Kruit.ppt> (last access: 12 June 2014).]
- Witte, J. C., A. R. Douglass, A. da Silva, O. Torres, R. Levy, and B. N. Duncan (2011), NASA A-Train and Terra observations of the 2010 Russian wildfires, *Atmos. Chem. Phys.*, *11*(17), 9287–9301, doi:10.5194/acp-11-9287-2011.
- Zhang, L., S. Gong, J. Padro, and L. Barrie (2001), A size-segregated particle dry deposition scheme for an atmospheric aerosol module, *Atmos. Environ.*, *35*(3), 549–560, doi:10.1016/S1352-2310(00)00326-5.
- Zhang, L., D. J. Jacob, E. M. Knipping, N. Kumar, J. W. Munger, C. C. Carouge, A. van Donkelaar, Y. X. Wang, and D. Chen (2012), Nitrogen deposition to the United States: Distribution, sources, and processes, *Atmos. Chem. Phys.*, *12*(10), 4539–4554, doi:10.5194/acp-12-4539-2012.
- Zhu, L., D. K. Henze, K. E. Cady-Pereira, M. W. Shephard, M. Luo, R. W. Pinder, J. O. Bash, and G.-R. Jeong (2013), Constraining U.S. ammonia emissions using TES remote sensing observations and the GEOS-Chem adjoint model, *J. Geophys. Res. Atmos.*, *118*, 3355–3368, doi:10.1002/jgrd.50166.